Cheryl Suwen Law, Siew Yee Lim and Abel Santos
Fine tuning of transmission features in nanoporous anodic alumina distributed Bragg reflectors
Proceedings of SPIE Nanophotonics Australasia 2017, 2018 / vol.10456, pp.1045659-1-1045659-15

Originally published at: http://dx.doi.org/10.1117/12.2282250

Fine tuning of transmission features in nanoporous anodic alumina distributed Bragg reflectors

Lim, Siew Yee, Law, Cheryl Suwen, Santos, Abel

Siew Yee Lim, Cheryl Suwen Law, Abel Santos, "Fine tuning of transmission features in nanoporous anodic alumina distributed Bragg reflectors," Proc. SPIE 10456, Nanophotonics Australasia 2017, 1045659 (2 January 2018); doi: 10.1117/12.2282250

SPIE.

Event: SPIE Nanophotonics Australasia, 2017, Melbourne, Australia

Fine Tuning of Transmission Features in Nanoporous Anodic Alumina Distributed Bragg Reflectors

Cheryl Suwen Law[1,2,3], Siew Yee Lim[1,2,3] and Abel Santos[1,2,3*]
[1]School of Chemical Engineering, The University of Adelaide, Adelaide, Australia
[2]Institute for Photonics and Advanced Sensing (IPAS), The University of Adelaide
[3]ARC Centre of Excellence for Nanoscale BioPhotonics (CNBP), The University of Adelaide, Adelaide
*abel.santos@adelaide.edu.au

ABSTRACT

This study introduces an innovative apodisation strategy to tune the filtering features of distributed Bragg reflectors based on nanoporous anodic alumina (NAA-DBRs). The effective medium of NAA-DBRs, which is modulated in a stepwise fashion by a pulse-like anodisation approach, is apodised following a logarithmic negative function to engineer the transmission features of NAA-DBRs. We investigate the effect of various apodisation parameters such as apodisation amplitude difference, anodisation period, current density offset and pore widening time, to tune and optimise the optical properties of NAA-DBRs in terms of central wavelength position, full width at half maximum and quality of photonic stop band. The transmission features of NAA-DBRs are shown to be fully controllable with precision across the spectral regions by means of the apodisation parameters. Our study demonstrates that an apodisation strategy can significantly narrow the width and enhance the quality of the characteristic photonic stop band of NAA-DBRs. This rationally designed anodisation approach based on the combination of apodisation and stepwise pulse anodisation enables the development of optical filters with tuneable filtering features to be integrated into optical technologies acting as essential photonic elements in devices such as optical sensors and biosensors.

Keywords: Nanoporous Anodic Alumina, Distributed Bragg Reflectors, Apodisation, Filtering Features, Stepwise Pulse Anodisation.

1. INTRODUCTION

Photonic crystals (PCs) are periodic micro/nanostructures that feature a regular distribution of refractive index (or dielectric constant), which can be arranged in either one, two or three dimensions[2-6]. PCs can modify the propagation of electromagnetic waves when photons travel across their structure due to the photonic stop bands that they possess.[7,8] The PCs' photonic stop bands allow or forbid the propagation of photons of certain wavelengths and these light–matter interactions can be precisely engineered by the PCs' structure. Among various fabrication techniques (i.e. lithography[9-13], wet chemical etching[14-15], fiber pulling[16], self-organisation[17,18] and electrochemical etching[19-22]), electrochemical oxidation of metals (anodisation) is a promising method to produce nanostructured PCs based on materials such as silicon, titanium and aluminium. Anodisation enables the in-depth engineering of the porosity of anodic oxides to produce multidimensional PCs with various refractive index profiles such as rugate filters[23-25], microcavities[26,27], waveguides[28-29] and distributed Bragg reflectors.[30,31]

Of all the materials produced by anodisation, nanoporous anodic alumina (NAA) – nanoporous anodic oxide produced by anodisation of aluminium – has superior properties in terms of chemical, mechanical and physical stability. Furthermore, the geometric features of nanopores in NAA can be controlled with versatility and precision by means of the anodisation parameters. NAA is an excellent platform to develop photonic structures since it features stable optical signals without additional passivation steps.[32] NAA can be produced by a cost-competitive, industrially scalable fabrication process, which enables the production of NAA with high degree of regularity, resolution and aspect ratio to guide, reflect, transmit, emit and enhance incident light by engineering its effective medium.[24,32-41] Recent studies have demonstrated that pulse-like anodisation strategies enable the development of a wide range of NAA PCs (i.e. distributed Bragg reflectors, gradient index filters, Fabry-pérot interferometer and microcavities). A careful selection of the anodisation conditions makes it possible to translate complex anodisation profiles such as pseudo-sinusoidal, sawtooth-

Nanophotonics Australasia 2017, edited by James W. M. Chon, Baohua Jia, Proc. of SPIE
Vol. 10456, 1045659 · © 2018 SPIE · CCC code: 0277-786X/18/$18 · doi: 10.1117/12.2282250

like, pseudo-stepwise and multi-sinusoidal into porosity modulations to engineer the NAA's effective medium in depth.[24,34-38,41-60] These NAA PCs possess unique characteristic photonic stop bands that are tuneable across the UV-visible-NIR spectrum.

This study aims to establish a rational anodisation approach to fabricate NAA-based distributed Bragg reflectors (NAA-DBRs) with well-resolved, distinctive and narrow photonic stop bands, where the conceptual illustration is presented in **Figure 1**. NAA-DBRs have a relatively wide photonic stop band with the presence of characteristics sidelobes on both sides of the band due to the sharp truncation of refractive index between adjacent layers within the PC structure.[61,62] These two characteristics of NAA-DBRs can be undesirable in applications that require precise optical filtering of light.[41,55-57] To suppress these redundant sidelobes, the contrast of refractive index profile can be modulated using smooth functions (e.g. Gaussian, sine and Kaiser windows) to minimise the refractive index contrast in NAA-DBRs. Furthermore, since the refractive index contrast of NAA-DBRs defines the width of the photonic stop bands, a low refractive index contrast can be translated into a reduction in the bandwidth.[61] Herein, we adopt an apodisation strategy to engineer and tune the characteristic photonic stop bands of NAA-DBRs. Stepwise pulse anodisation (SPA), as shown in **Figure 1a** (Left), is used to produce NAA-DBRs featured with a distribution of effective refractive index that follows a stepwise profile along the nanopores (**Figure 1b** - left). A logarithmic negative apodisation function is employed to apodise the SPA (**Figure 1a** – right) in order to produce NAA-DRBs with well-resolved and high quality photonic stop bands. Different apodisation parameters, namely anodisation amplitude difference, anodisation period, current density offset and pore widening time are systematically manipulated to assess their effect on the features of the characteristics photonic stop bands of NAA-DBRs (**Figure 1c**). This work further advances NAA-based PCs technology demonstrating that anodisation can provide a precise control over the photonic stop bands, unraveling exciting and promising potential applications in optical sensing, optical filters and photonic devices.

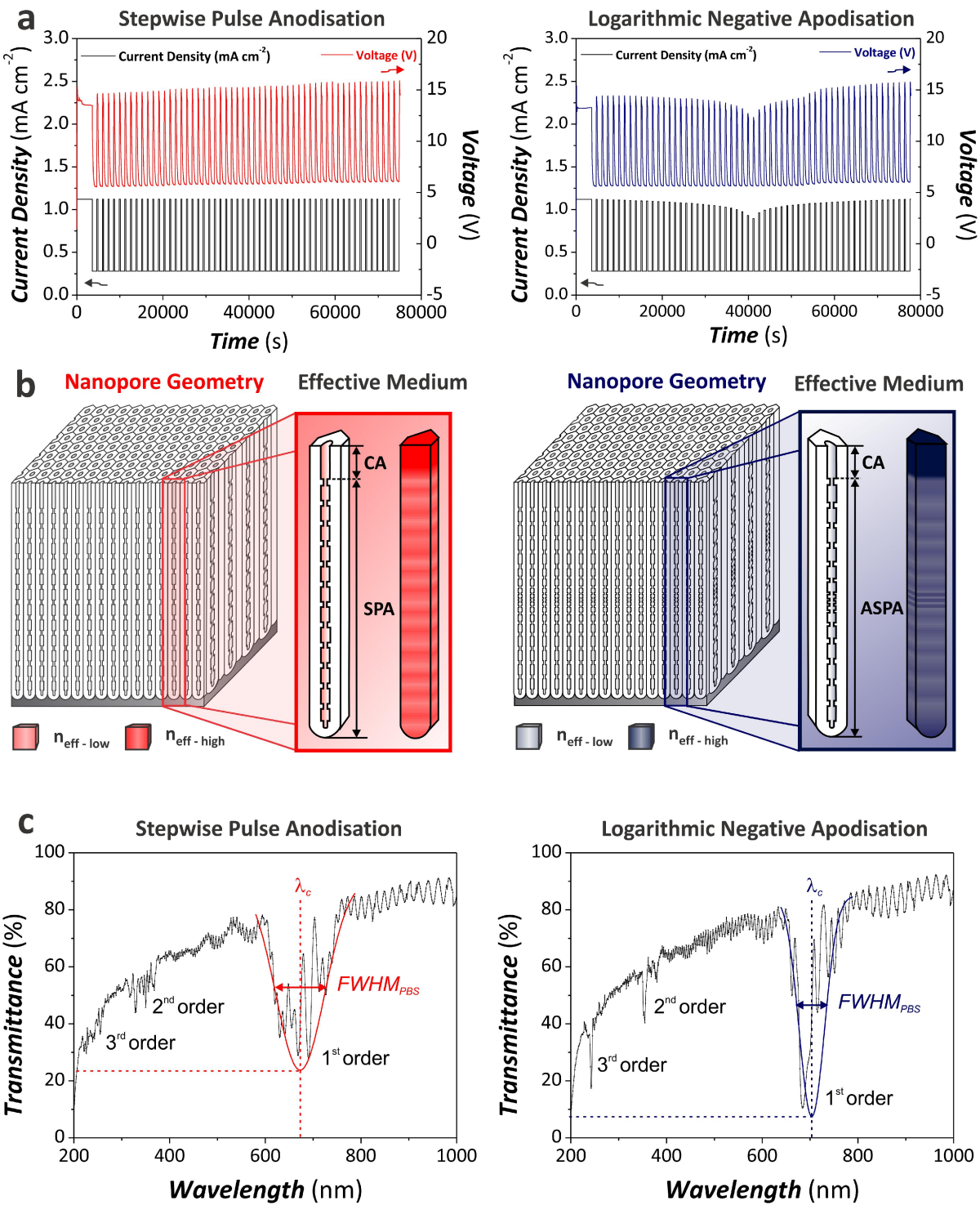

Figure 1. Illustrative concept of fabrication and characterisation of nanoporous anodic alumina distributed Bragg reflectors (NAA-DBRs). (a) Example of stepwise pulse anodisation profile used to produce NAA-DBRs (Right – No apodisation; Left- Logarithmic negative apodisation) (b) Schematic diagram of nanoporous structure of NAA-DBRs with effective medium approximation under non-apodisation (Right) and apodisation (Left) condition. (c) Representative transmission spectra of NAA-DBRs with definitive characteristic parameters (Right – No apodisation; Left- Logarithmic negative apodisation).

2. METHODOLOGY

2.1 Fabrication of NAA-DBRs

Nanoporous anodic alumina-based distributed Bragg reflectors (NAA-DBRs) were produced by apodised stepwise pulse anodisation (ASPA) under galvanostatic conditions. 1.5 x 1.5 cm aluminium (Al) square chips were prepared and cleaned under sonification in ethanol and distilled water for 15 min each, then dried under air stream. Cleaned Al substrates were electropolished in a mixture of ethanol (EtOH) and perchloric acid 4:1 (v:v) at 20 V and 5 ℃ for 3 min. Electropolished chips were then anodised in an electrochemical reactor at -1 ℃ using aqueous solution of 1.1.M of sulphuric acid with 25 v% of EtOH as electrolyte. Note that the anodisation temperature was kept constant throughout the process. The galvanostatic anodisation process started with a constant step at a current density of 1.12 mA cm^{-2} for 1 h to allow the formation of a thin nanoporous layer that facilitates a homogenous pore growth rate prior to ASPA. The anodisation profile was then set to stepwise pulse mode modified with logarithmic negative apodisation function. ASPA profiles were produced by a custom-designed Labview®-based software based on Eq.1.

$$J(t) = 2A_J(t) + J_{offset} \tag{1}$$

where $A_J\ (t)$ is time-dependent current density amplitude based on logarithmic negative apodisation function. Logarithmic negative apodised amplitude is expressed as a function of time, as shown in Eqs. 2 and 3.

For $t \leq t_{an}/2$

$$A(t)_J = A_{\max} + \left(\frac{A_{\min} - A_{\max}}{\log\left(\frac{t_{an}}{2} + 10\right) - 1} \right).\left(\log(t+10) - 1\right) \tag{2}$$

For $t > t_{an}/2$

$$A(t)_J = \left(\frac{A_{\max} - A_{\min}}{\log(t_{an} + 10) - \log\left(\frac{t_{an}}{2} + 10\right)} \right).\left(\log(t+10) - \log\left(\frac{t_{an}}{2} + 10\right) \right) + A_{\min} \tag{3}$$

where A_{max} and A_{min} are the maximum and minimum amplitudes, whereas t_{an} is the total anodisation time at ASPA.

In order to achieve fine tuning of transmission features of NAA-DBRs, several apodisation parameters, namely anodisation amplitude difference (ΔA_J), anodisation period (T_p), current density offset (J_{offset}) and pore widening time (t_{pw}) were systematically modified from 0 to 0.42 mA cm^{-2} with a step size of 0.21 mA cm^{-2}; from 1100 to 1500 s with a step size of 200 s; from 0.14 to 0.42 mA cm^{-2} with a step size of 0.14 mA cm^{-2}; and from 0 to 6 min with an interval of 2 min, respectively.

2.2 Optical characterisation

To selectively dissolve the remaining aluminium substrate from the back side of these aluminium chips, NAA-DBRs were subjected to chemical etching in an etching cell with a saturated solution of $HCl/CuCl_2$ using an etching mask with a circular window of 5 mm in diameter. Etched NAA-DBRs were then pore widened in an aqueous solution of 5 wt % H_3PO_4 at 35 ^oC for t_{pw} of 0, 2, 4, and 6 min and optically characterised. The features of the photonic stop band (PSB) of etched NAA-DBRs (position and full width at half maximum – FWHM) were then assessed by measuring their transmission spectra by UV-visible-NIR spectroscopy (Cary 5000, Agilent, USA) for the wavelength range 200–1500 nm at normal incidence (i.e. $\theta = 0^o$) with a resolution of 1 nm. The interferometric colour displayed by NAA-DBRs was

evaluated by digital images acquired using a Canon EOS 700D digital camera equipped with a Tamron 90 mm F2.8 VC USD macro mount lens with autofocus function under natural illumination.

2.3 Structural characterisation

The structural properties of NAA-DBRs were characterised by a field emission gun scanning electron microscope (FEG-SEM FEI Quanta 450). The acquired SEM images were analysed using ImageJ (public domain program developed at RSB of the NIH).

3. RESULTS AND DISCUSSION

3.1 Fabrication and structural characterisation of NAA-DBRs

NAA-DBRs were fabricated by stepwise pulse anodisation (SPA), where the current density was pulsed between high and low current density values in a stepwise fashion after a short constant anodisation (CA) step, as illustrated in **Figure 1a** – left. The nanoporous structure of NAA-DBRs was engineered in depth according to stepwise anodisation waves, yielding stacks of NAA layers with stepwise modulated porosity (**Figure 2b**). As denoted by the white arrows in **Figure 2b**, the length between consecutive NAA layers, which defines the period length (L_{Tp}), corresponds to each stepwise pulse in the anodisation profile and it was found to be 211 ± 6 nm for NAA-DBR produced at an anodisation period of 1300 s. On the other hand, apodised NAA-DBRs were produced by apodising the SPA profile using a logarithmic negative function (**Figure 1b**). The in-depth porosity of NAA-DBRs, as described in **Figure 1b** – left, was directly proportional to the apodisation current density during anodisation.

3.2 Effect of apodisation amplitude difference on the transmission features of NAA-DBRs

Figure 1c shows representative transmission spectra of non-apodised and logarithmic negative apodised NAA-DBRs fabricated under the same anodisation conditions. From the analysis of **Figure 1c**, it is revealed that both non-apodised and apodised NAA-DBRs display not only first order PSB in the range of 650–750 nm, but also second and third order PSBs in the range of 350–400 nm and 250–300 nm, respectively. The intensity of the first order PSB is greater than that of second and third order PSBs. They also display significant ripples in their transmission spectra due to interference fringes. However, the PSB of apodised NAA-DBRs has a narrower width with minimised sidelobes as compared to that of non-apodised NAA-DBRs. The application of apodisation enhances the intensity of PSB in addition to improving the resolution of the PSB, in particular the second and third orders PSBs, resulting in well-resolved and sharper bands. The transmission spectra of non-apodised and apodised NAA-DBRs as a function of t_{pw} in **Figures 2c and d** show the same trend in the effect of t_{pw} on the position of the PSB across the UV-visible-NIR range, where it undergoes a blue shift (i.e. first, second and third order) as the nanoporous structure of NAA-DBRs is widened with increasing t_{pw}. These results are in good agreement with previous studies.[40,57,60] To widen the nanopores of NAA-DBRs enhances the contrast of porosity between consecutives layer of NAA due to the existing gradient dissolution rate between NAA layers produced at different current density levels, resulting in a decrease of the overall effective refractive index of NAA-DBRs. This in turn shifts the position of PSB towards regions of shorter wavelength[40,63]. It was also observed that an increase in t_{pw} results in the broadening of the PSB, as observed in **Figures 2c and d**.

For non-apodised NAA-DBRs, the intensity of first order characteristic PSB increases through pore widening treatment. However, the intensity of second and third order PSB is not affected by pore widening process, as shown in **Figure 2c**. The transmittance baseline, on the other hand, decreases as t_{pw} increases, which can be attributed to the over etching of the nanopores and light scattering effects by the PC structure, as reported in previous studies.[40] Similar to non-apodised NAA-DBRs, the intensity of the characteristic first order PSB of apodised NAA-DBRs increases with increasing t_{pw}. However, in contrast to non-apodised NAA-DBRs, the increase in the intensity of PSB for apodised NAA-DBRs is found to be less significant. Furthermore, a decrease in the intensity of second order and third order PSBs is observed as apodised NAA-DBRs are etched at a longer t_{pw}. The transmittance baseline of apodised NAA-DBRs is maintained despite the increasing t_{pw} from 0 to 4 min (**Figure 2d**). Furthermore, our analysis reveals that apodised NAA-DBRs feature enhanced intensity of the characteristics PSBs as compared to that of pore widening treatment. Thus apodisation is an effective means to tune the width as well as enhancing the intensity of characteristic PSBs.

As displayed in **Figure 1c**, it is observed that the characteristics PSB of non-apodised and apodised NAA-DBRs is similar to a bell-shaped curve, which can be approximated to a Gaussian curve with a central peak wavelength at its

maximum (λ_c) and its full width at half maximum ($FWHM_{PSB}$). λ_c denotes the location of the first order characteristic PSB in the UV-visible-NIR spectrum, whereas $FWHM_{PSB}$ indicates the width of the characteristic PSB. These two parameters, λ_c and $FWHM_{PSB}$, are used to define the quality factor of the PSB (Q_{PSB}) in NAA-DBRs, where a high quality of characteristic stop band is represented by a high value of Q_{PSB}. The expression that correlates λ_c and $FWHM_{PSB}$ to Q_{PSB} is shown in Eq. 4.

$$Q_{PSB} = \frac{\lambda_c}{FWHM_{PBS}} \tag{4}$$

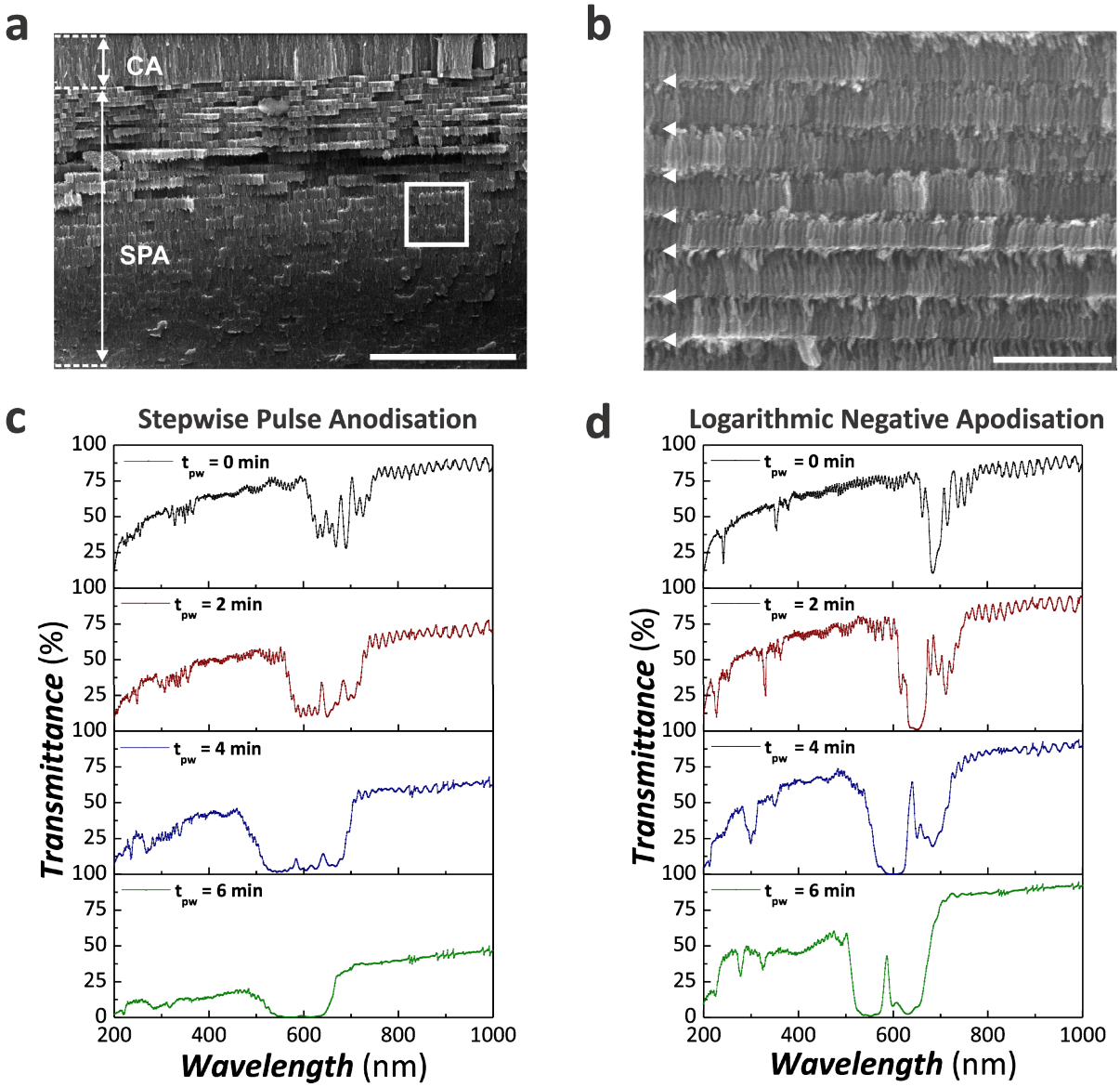

Figure 2. Structural and optical characterisation of nanoporous anodic alumina distributed Bragg reflectors. (a) SEM image showing the cross section of NAA-DBRs produced at ΔA_J = 0 mA cm^{-2}, T_p = 1300 s, J_{offset} = 0.28 mA cm^{-2} and t_{pw} = 6 min (scale bar = 5 µm). (b) Magnified view of white square in (a) showing stacks of NAA layers with the arrows denoting the period length (L_{Tp}) (scale bar = 500 nm). (c) Transmission spectra of NAA-DBRs (ΔA_J = 0 mA cm^{-2}, T_p = 1300 s, J_{offset} = 0.28 mA cm^{-2}) at different t_{pw}. (d) Transmission spectra of logarithmic negative apodised NAA-DBRs (ΔA_J = 0.21 mA cm^{-2}, T_p = 1300 s, J_{offset} = 0.28 mA cm^{-2}) as a function of t_{pw}.

The apodisation amplitude difference (ΔA_J) was systematically modified from 0 to 0.42 mA cm^{-2} with an interval of 0.21 mA cm^{-2} to unveil the effect of this fabrication parameter on the optical properties of NAA-DBRs in terms of λ_c, $FWHM_{PSB}$, Q_{PSB} and interferometric colour. Note that NAA-DBRs produced at ΔA_J = 0 mA cm^{-2} correspond to non-apodised NAA-DBRs, while NAA-DBRs produced at ΔA_J = 0.21 and 0.42 mA cm^{-2} are logarithmic negative apodised with ΔA_J of respective values. The results obtained are shown in **Figure 3** and they are based on the first order PSB as it plays a more significant role on governing the optical properties of NAA-DBRs as compared to the second and third order PSBs. **Figure 3a** shows the correlation of λ_c to ΔA_J for NAA-DBRs at different t_{pw}, where λ_c is observed to be located within the visible range. When ΔA_J is increased from 0 to 0.21 mA cm^{-2}, there is a slight red shift in λ_c but a slight blue shift when ΔA_J is further increased to 0.42 mA cm^{-2}. It is worthwhile to note that the magnitude of this shift is minimal and thus ΔA_J has a weak influence on λ_c regardless of t_{pw}. Compared to ΔA_J, the effect of t_{pw} on λ_c is more significant as the magnitude of this shift in λ_c is greater. As aforementioned, an increase in t_{pw} induces a blue shift in λ_c. This trend is also observed in **Figure 3a**, where λ_c is shifted to shorter wavelengths as t_{pw} increases. This is observed for all NAA-DBRs produced with different ΔA_J.

λ_c establishes the interferometric colour displayed by NAA-DBRs as λ_c indicates the wavelength at which light is reflected more efficiently by the PC structure. **Figure 3b** depicts the colour properties of NAA-DBRs as a function of ΔA_J and t_{pw}. These NAA-DBRs display colours such as red, orange and yellow as their λ_c are located within the visible range. Non-apodised NAA-DBRs (ΔA_J = 0 mA cm^{-2}) display more distinct colour with stronger intensity as they reflect light more efficiently (i.e. broader band of wavelengths), which is consistent with the results obtained in previous study.[58] On the contrary, the colour of apodised NAA-DBRs are paler than that of non-apodised NAA-DBRs, the brightness of which is observed to decrease as ΔA_J increases. As the difference between minimum and maximum anodisation amplitude is greater, the period length varies to a greater extent in depth along the nanopores. As a result, light is reflected more selectively but in a less efficient manner. For instance, the interferometric colour of apodised NAA-DBRs with ΔA_J = 0 mA cm^{-2} and t_{pw} = 4 min is a blend of light yellow and pale green. The blue shift in λ_c due to an increase in t_{pw} is also reflected in the interferometric colour change of these NAA-DBRs from red-orange to yellow-green when λ_c shifts from the upper range (i.e. when t_{pw} = 0 and 2 min) to mid-range (i.e. when t_{pw} = 4 and 6 min) of the visible spectrum.

The contour map in **Figure 3c** illustrates the effect of ΔA_J and t_{pw} on $FWHM_{PSB}$ of the characteristic bands of NAA-DBRs. The PSBs of NAA-DBRs can be characterised in terms of their $FWHM_{PSB}$, upon which a more selective and sensitive NAA-DBRs have narrow characteristic stop bands with a low value of $FWHM_{PSB}$.[58] ΔA_J has a strong influence on $FWHM_{PSB}$ in non-apodised NAA-DBRs as the field lines at ΔA_J = 0 mA cm^{-2} are relatively close. The distance between the field lines increases as ΔA_J increases to 0.42 mA cm^{-2}, inferring that a greater difference in anodisation amplitude has a weaker effect on $FWHM_{PSB}$. The width of the characteristic PSB of NAA-DBRs decreases as ΔA_J approaches 0.21 mA cm^{-2} from 0 and 0.42 mA cm^{-2}, suggesting that ΔA_J = 0.21 mA cm^{-2} is the optimum apodising parameter in producing narrow stop bands with a $FWHM_{PSB}$ of 32 ± 1 nm. On the contrary, the non-apodised NAA-DBRs (ΔA_J = 0 mA cm^{-2}) counterpart has a $FWHM_{PSB}$ of 130 ± 1 nm, which is ~4 times wider than that of apodised NAA-DBRs. Thus apodisation is demonstrated to be an effective approach in tuning the width of the PSB as a lower $FWHM_{PSB}$ is favourable in producing high quality characteristic stop bands. The equidistant field lines at short t_{pw} (0 and 2 min) as well as the wide field lines at longer t_{pw} (4 and 6 min) reveal that the $FWHM_{PSB}$ has a stronger dependency at shorter t_{pw}. $FWHM_{PSB}$ increases as t_{pw} increases, in spite of the varying ΔA_J.

With the determined λ_c and $FWHM_{PSB}$, the quality of characteristic PSBs (Q_{PSB}) is analysed using Eq. 4 and the distribution of Q_{PSB} as a function of ΔA_J and t_{pw} for apodised and non-apodised NAA-DBRs is shown in **Figure 3d**. The colour fields in **Figure 3d** concentrate at the region of t_{pw} = 0 to 2 min and the distance between the field lines decreases with decreasing t_{pw}. In general, Q_{PSB} increases as t_{pw} decreases and this suggests that pore widening has a negative effect in producing NAA-DBRs with high quality characteristic PSBs. The application of apodisation has a positive impact on Q_{PSB}, as described by the decreasing field line distances when ΔA_J increases from 0 to 0.21 mA cm^{-2}. Further increase of ΔA_J to 0.42 mA cm^{-2} has a slightly less significant effect on Q_{PSB}, denoted by the wider field line distances. This yields a local maximum of Q_{PSB} = 21.3 ± 0.6 at ΔA_J = 0.21 mA cm^{-2} and t_{pw} = 0 min, producing logarithmic negative apodised NAA-DBRs with high quality characteristic PSB. This is ~4.1 times greater than the Q_{PSB} of non-apodised NAA-DBRs (i.e. ΔA_J = 0 mA cm^{-2} and t_{pw} = 0 min) with a value of 5.1 ± 0.2.

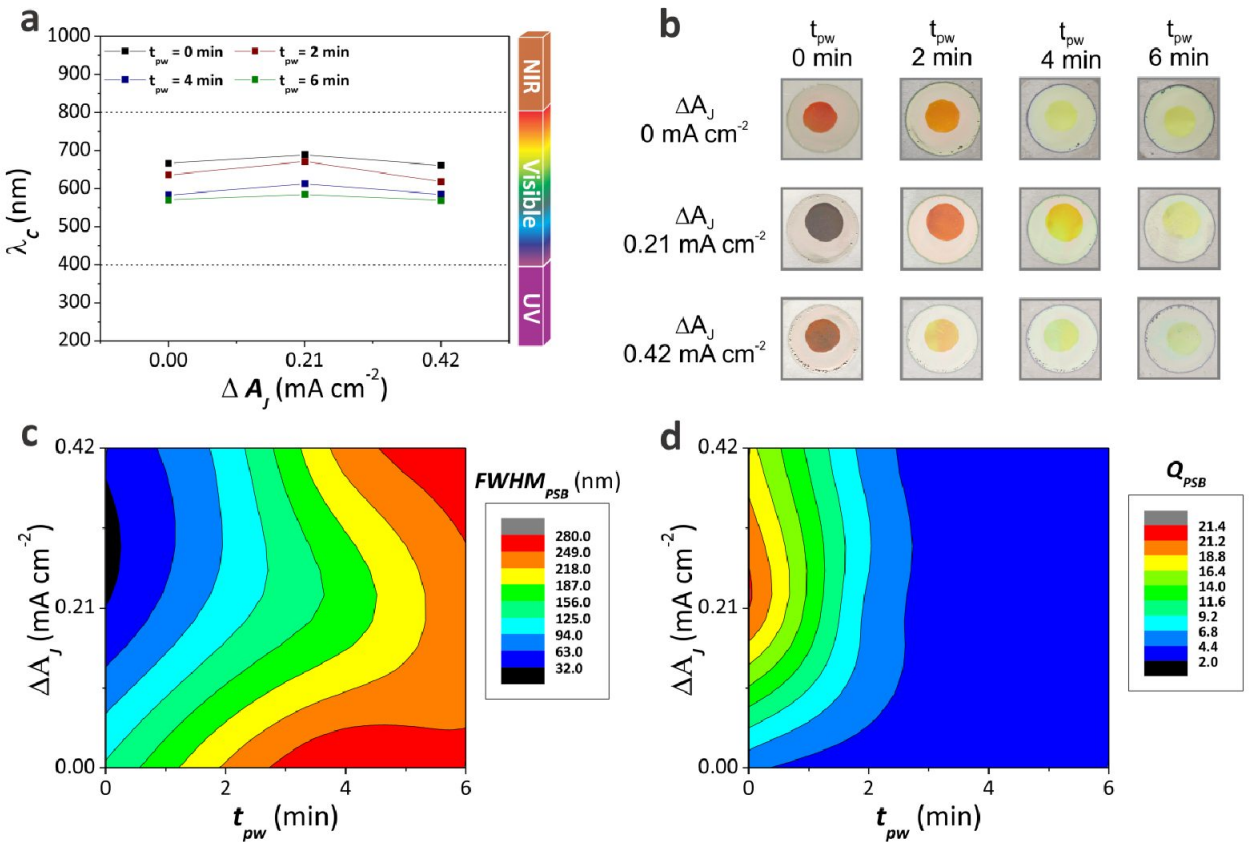

Figure 3. Effect of ΔA_J on the transmission features of NAA-DBRs. (a) Correlation between ΔA_J and the position of central PSB of apodised NAA-DBRs at different t_{pw}. (b) Digital photos of apodised NAA-DBRs (diameter = 1cm) as a function of ΔA_J and t_{pw}. (c) Contour plot showing the distribution of $FWHM_{PSB}$ by the manipulation of ΔA_J and t_{pw}. (d) Contour plot describing the dependence of Q_{PSB} on ΔA_J and t_{pw}. (Note: T_p and J_{offset} were fixed at 1300 s and 0.28 mA cm^{-2}, respectively).

3.3 Effect of anodisation period on the transmission features of NAA-DBRs

As shown in the previous section, NAA-DBRs apodised with ΔA_J = 0.21 mA cm^{-2} are demonstrated to exhibit high quality characteristic PSBs. By keeping ΔA_J constant at 0.21 mA cm^{-2}, the anodisation period (T_p) was modified from 1100 to 1500 s with an interval of 200 s to study the effect of T_p on the transmission features of logarithmic negative apodised NAA-DBRs in terms of λ_c, interferometric colours, $FWHM_{PSB}$ and Q_{PSB}. The transmission spectra of apodised NAA-DBRs produced at different T_p show first, second and third order characteristic PSBs, similar to that in **Figure 2d**. **Figure 4a** shows how the position of λ_c for the first order PSB changes with T_p and t_{pw} across UV-visible-NIR spectrum. For all T_p, the central wavelength of apodised NAA-DBRs is located within the visible range of the spectrum. A linear relationship between T_p and λ_c is established, where the longer the anodisation period, the longer the central wavelength is positioned at. For example, λ_c of as-produced apodised NAA-DBRs with T_p of 1100 s is at 570 ± 1 nm and λ_c shifts to 780 ± 1 nm when T_p increases to 1500 nm. This result is in good agreement with previous studies.[57,58,60] As the anodisation period determines the period length within the nanoporous structure of apodised NAA-DBRs, the longer the anodisation period, the longer the length of NAA layers between consecutive stepwise pulses, resulting in the reflection of light at longer wavelengths. By further increase the anodisation period (i.e. T_p > 1500 s), the position of λ_c can be engineered in the NIR region. T_p is an effective parameter to achieve versatile tuneability of λ_c across the spectral regions. Increasing t_{pw} has the same effect (i.e. blue shift) on λ_c of apodised NAA-DBRs produced with different T_p as to that of different ΔA_J.

Apodised NAA-DBRs display vivid interferometric colours when λ_c is located within the visible range (500 to 800 nm). However, λ_c of apodised NAA-DBR with T_p = 1500 s and t_{pw} = 0 min is located at 780 nm, which is relatively close to the NIR region, and thus these NAA-DBRs are transparent (black colour denoted by the background). There is a red shift in the interferometric colour of apodised NAA-DBRs with T_p from 1100 to 1500 s as depicted in **Figure 4b**. For

example, at t_{pw} = 4 min, apodised NAA-DBRs display turquoise (i.e. λ_c = 520 nm) at T_p = 1100 s and the colour changes to yellow and then orange as λ_c shifts from 600 to 650 nm. The blue shift in λ_c that results from the increase in t_{pw} is also established by the interferometric colour change of apodised NAA-DBRs. However, it is worth nothing that the colour change of apodised NAA-DBRs from the effect of t_{pw} is not as significant as the effect of T_p. Furthermore, the colour intensity of these apodised NAA-DBRs is fairly strong as they are apodised with a moderate value of ΔA_J (i.e. 0.21 mA cm^{-2}).

The analysis of $FWHM_{PSB}$ as a function of T_p and t_{pw} is presented **Figure 4c**. As denoted by the relative wide colour field and distant field lines, $FWHM_{PSB}$ has a relatively weak dependency on T_p. However, a general trend is observed between $FWHM_{PSB}$ and T_p. $FWHM_{PSB}$ increases with T_p, thus apodised NAA-DBRs produced with longer T_p exhibit wider characteristic PSBs due to the increased period length within the PC structure. However, apodised NAA-DBRs with t_{pw} = 6 min show an opposite effect, where $FWHM_{PSB}$ increases as T_p decreases. This might be due to the over-etching after pore widening treatment. For the effect of t_{pw} on $FWHM_{PSB}$, $FWHM_{PSB}$ of apodised NAA-DBRs has a stronger dependence on longer t_{pw}, as conveyed by the shorter field line distances at t_{pw} = 4 and 6 min. Apodised NAA-DBRs produced with various T_p show an increase in $FWHM_{PSB}$ as they are pore widened. This treatment increases the diameter of nanopores of apodised, resulting in wider PSB with higher values of $FWHM_{PSB}$. Therefore, t_{pw} has a greater influence on $FWHM_{PSB}$ than that of T_P. A local minima of $FWHM_{PSB}$ = 32 ± 1 nm is identified in the colour map when the fabrication parameters are set at T_p = 1300 s and t_{pw} = 0 min. Apodised NAA-DBRs produced at these parameters exhibit a narrow characteristic PSB.

The correlation between Q_{PSB} and T_p and t_{pw} is presented in the contour map in **Figure 4d**. The colour field is dense with close field lines at the region of t_{pw} = 0 and 2 min, but the distance between the field lines in the map increases with t_{pw}, denoting that the dependence of Q_{PSB} of apodised NAA-DBRs on t_{pw} is weaker as t_{pw} increases. Furthermore, the quality of characteristic PSB of apodised NAA-DBRs is worsened as they are pore widened, which can be predicted from the values of $FWHM_{PSB}$ based on the inversely proportional relationship between $FWHM_{PSB}$ and Q_{PSB}. Further modification of T_p has a negative effect on enhancing the Q_{PSB} of apodised NAA-DBRs with $t_{pw} \geq 4$ min. Pore widening treatment broadens the characteristic PSB of apodised NAA-DBRs, thus decreasing the Q_{PSB}. The distance between the field lines decreases as T_p is modified from 1100 and 1500 s, suggesting the dependency of Q_{PSB} on T_p increases as T_p approaches to 1300 s. This gives rise to a local maximum with a value of Q_{PSB} of 21.3 ± 0.6 at T_p = 1300 s and t_{pw} = 0 min. The colour fields denote that fabrication at shorter T_p produces apodised NAA-DBRs with better Q_{PSB} than those at longer T_p. Unlike $FWHM_{PSB}$, which depends more on t_{pw} than on T_p, Q_{PSB} of apodised NAA-DBRs shows a stronger dependency on T_p rather than t_{pw}.

3.4 Effect of current density offset on the transmission features of NAA-DBRs

To achieve precise tuning of the transmission features, apodised NAA-DBRs were fabricated at different current density offset (J_{offset}): 0.14, 0.28 and 0.42 mA cm^{-2}. Their transmission spectra and digital photos were measured and analysed, and the results obtained are compiled in **Figure 5**. The correlation between J_{offset} and λ_c of apodised NAA-DBRs at different t_{pw} for the first order PSB is presented in **Figure 5a**. Apodised NAA-DBRs produced at J_{offset} of 0.14 and 0.28 mA cm^{-2} have their characteristics λ_c located within the visible range, whereas λ_c of those at J_{offset} = 0.42 mA cm^{-2} is in the NIR range. λ_c of apodised NAA-DBRs is shown to have a linear relationship with J_{offset}, the higher J_{offset} is the longer λ_c, thus red-shifting λ_c towards the NIR region. This result is consistent with the results obtained in previous studies.[60] It is also observed that the shift in λ_c is greater when J_{offset} increases from 0.28 to 0.42 mA cm^{-2} in spite of the different t_{pw}. The manipulation of t_{pw} has shown the same effect on λ_c; longer t_{pw} induces a blue shift in λ_c due to the decrease in the overall refractive index of apodised NAA-DBRs and the enhanced porosity contrast. The position of λ_c of apodised NAA-DBRs is more affected by the manipulation of J_{offset} than t_{pw}, as established by the magnitude of the shift in λ_c. J_{offset} are demonstrated to be an effective parameter to precisely engineer the transmission PSB of apodised NAA-DBRs across the entire UV-visible-NIR spectrum.

The digital photos showing the interferometric colour of apodised NAA-DBRs produced at different J_{offset} and t_{pw} are shown in **Figure 5b**. Apodised NAA-DBRs fabricated at high J_{offset} (i.e. 0.42 mA cm^{-2}) are found to be transparent as they reflect light of wavelength in the NIR region. On the contrary, apodised NAA-DBRs with J_{offset} of 0.14 and 0.28 mA cm^{-2} display vivid interferometric colours, such as blue, green, yellow and orange, which correspond to their respective first order characteristic PSB in the visible range. The red shift in λ_c due to increasing J_{offset} is also described by the colour change in apodised NAA-DBRs. Apodised NAA-DBRs of J_{offset} = 0.14 mA cm^{-2} has displayed blue-green color as their λ_c are in the mid-range of the visible spectrum, and the colour changes to yellow-red when J_{offset} is increased to 0.28 mA cm^{-2}. Further increase of J_{offset} to 0.42 mA cm^{-2} induces a greater red shift in λ_c towards the NIR range. A blue shift in

the interferometric colours of apodised NAA-DBRs is observed with t_{pw}. The colour displayed by these apodised NAA-DBRs are fairly intense as they are fabricated at moderate $\Delta A_J = 0.21$ mA cm^{-2}.

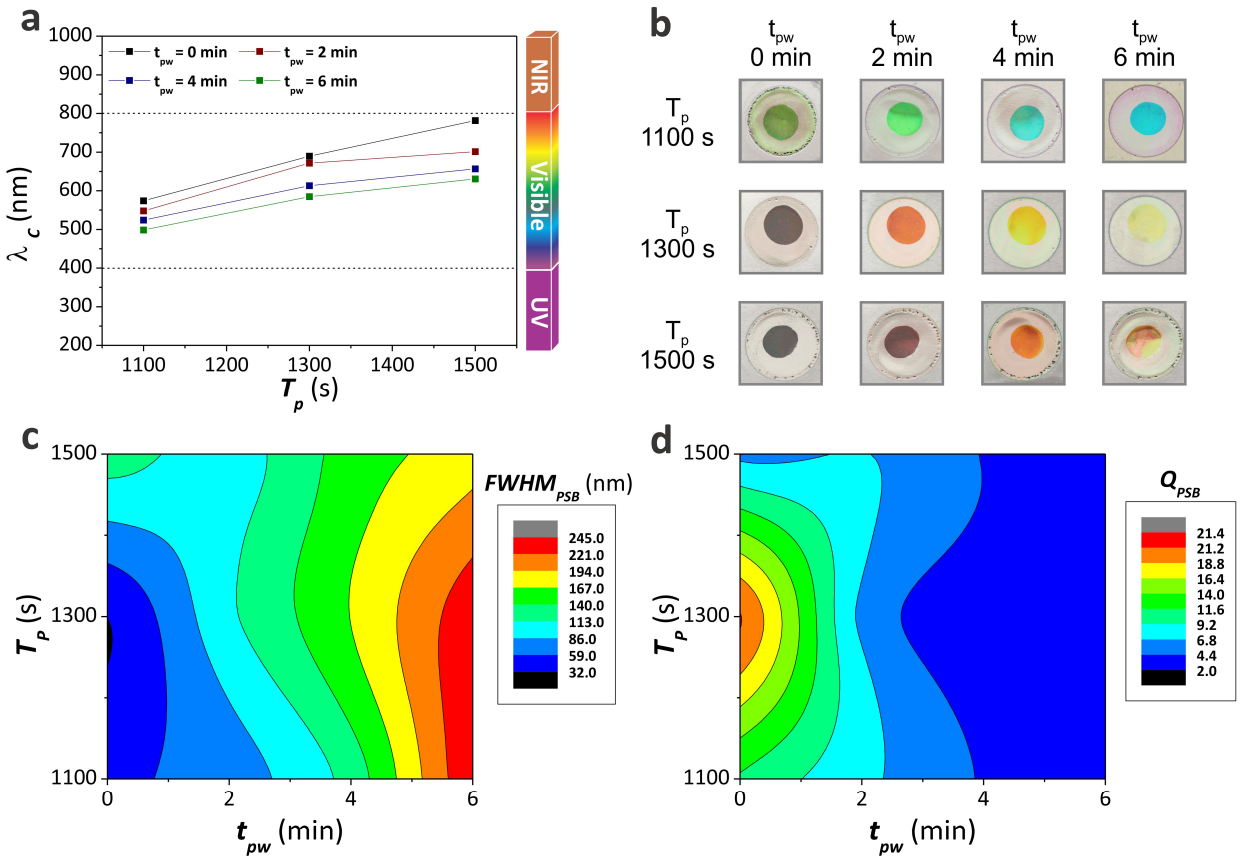

Figure 4. Effect of T_p on the transmission features of logarithmic negative apodised NAA-DBRs. (a) A linear relationship between T_p and λ_c of NAA-DBRs for different t_{pw}. (b) Digital photos of apodised NAA-DBRs of 1 cm diameter illustrating their interferometric colours as a function of T_p and t_{pw}. (c) Contour map showing the dependence of $FWHM_{PSB}$ on T_p and t_{pw}. (d) Contour map describing the effect of T_p and t_{pw} on Q_{PSB}. (Note: ΔA_J and J_{offset} were fixed at 0.21 and 0.28 mA cm^{-2})

Figure 5c shows the distribution of $FWHM_{PSB}$ in terms of J_{offset} and t_{pw}. The closer and equidistant colour lines in the bottom left region of the map indicate that $FWHM_{PSB}$ of apodised NAA-DBRs has a slightly stronger dependence at low J_{offset} and short t_{pw}. Other than that, the rest of the map is of wide colour field and field lines, implying the weak correlation of $FWHM_{PSB}$ to J_{offset} and t_{pw}. However, when comparing the effect of J_{offset} and t_{pw} on $FWHM_{PSB}$, t_{pw} plays a more significant role in $FWHM_{PSB}$ of apodised NAA-DBRs, as described by the closer field lines as well as the colour fields across the x-axis direction (i.e. blue to red). As a consequence from the increment of t_{pw} in the pore widening treatment of apodised NAA-DBRs, their characteristics PSB broadens with increasing $FWHM_{PSB}$, which may not be desirable for applications requiring high sensitivity. The effect of J_{offset} generally causes a slight increase in $FWHM_{PSB}$, as illustrated by the distribution of colour fields along the y-axis. Nonetheless, apodised NAA-DBRs produced at J_{offset} = 0.28 mA cm^{-2} and $t_{pw} = 0$ min have the narrowest characteristic PSB with a $FWHM_{PSB}$ of 32 ± 1 nm, as identified in the colour map.

Q_{PSB} of apodised NAA-DBRs are determined through their correlation to λ_c and $FWHM_{PSB}$, established by Eq. 4, and the results as a function of J_{offset} and t_{pw} are summarised in **Figure 5d**. Similar to **Figures 3d and 4d**, the colour fields concentrate on the region of $t_{pw} < 2$ min. From the closer distance between the field lines at $t_{pw} \leq 2$ min than that of $t_{pw} \geq 2$ min, it is apparent that the dependency of Q_{PSB} on t_{pw} increases as t_{pw} decreases from 6 to 0 min. Furthermore, the evolution of colour field across the x-axis suggests that shorter t_{pw} favours the production of apodised NAA-DBRs with high quality characteristic PSBs. In term of the effect of J_{offset}, by focusing on the region of $t_{pw} = 0$ min, the colour field between 0.14 and 0.28 mA cm^{-2} are denser with closer field lines as compared to the region between 0.28 and 0.42 mA

cm^{-2}. This reveals that Q_{PSB} has a stronger dependency on $J_{offset} \leq 0.28$ mA cm^{-2} as compared to $J_{offset} \geq 0.28$ mA cm^{-2}. This also denotes that apodised NAA-DBRs with $J_{offset} = 0.14$ mA cm^{-2} have a greater Q_{PSB} than those of $J_{offset} = 0.42$ mA cm^{-2}, with a local maximum of Q_{PSB} of 21.3 ± 0.6 at $J_{offset} = 0.28$ mA cm^{-2} and $t_{pw} = 0$ min. On the whole, the contour map demonstrates that J_{offset} has a more substantial effect on Q_{PSB} of apodised NAA-DBRs as compared to t_{pw}. However, pore widening of apodised NAA-DBRs with prolonged t_{pw} has a stronger effect in decreasing Q_{PSB}, despite the manipulation of J_{offset} for the enhancement of the quality of characteristic PSBs.

The comparison between **Figures 3a, 4a and 5a** has revealed that the modification of T_p and J_{offset} can be used to shift λ_c across the entire UV-visible-NIR spectrum efficiently and effectively. This also allows the tuning of the interferometric colours displayed by NAA-DBRs, which is a suitable feature to develop versatile photonic nanotools for visual sensing. In the case of Q_{PSB}, ΔA_J plays a more significant role in the determination of Q_{PSB}, as denoted by the closer field lines in the colour field when **Figures 3d, 4d and 5d** are compared. Regarding $FWHM_{PSB}$, the wide colour fields in **Figures 3c, 4c and 5c** described the relatively weak dependency of $FWHM_{PSB}$ on ΔA_J, T_p and J_{offset}, instead $FWHM_{PSB}$ correlates more to t_{pw}. Another observation is that the combination of apodisation with stepwise pulse anodisation has shown a better result in minimising the bandwidth and maximising the quality of PSB (Q_{PSB} = 21.3 ± 0.6) as compared to sinusoidal pulse anodisation (Q_{PSB} = 4.6 ± 0.4).[58]

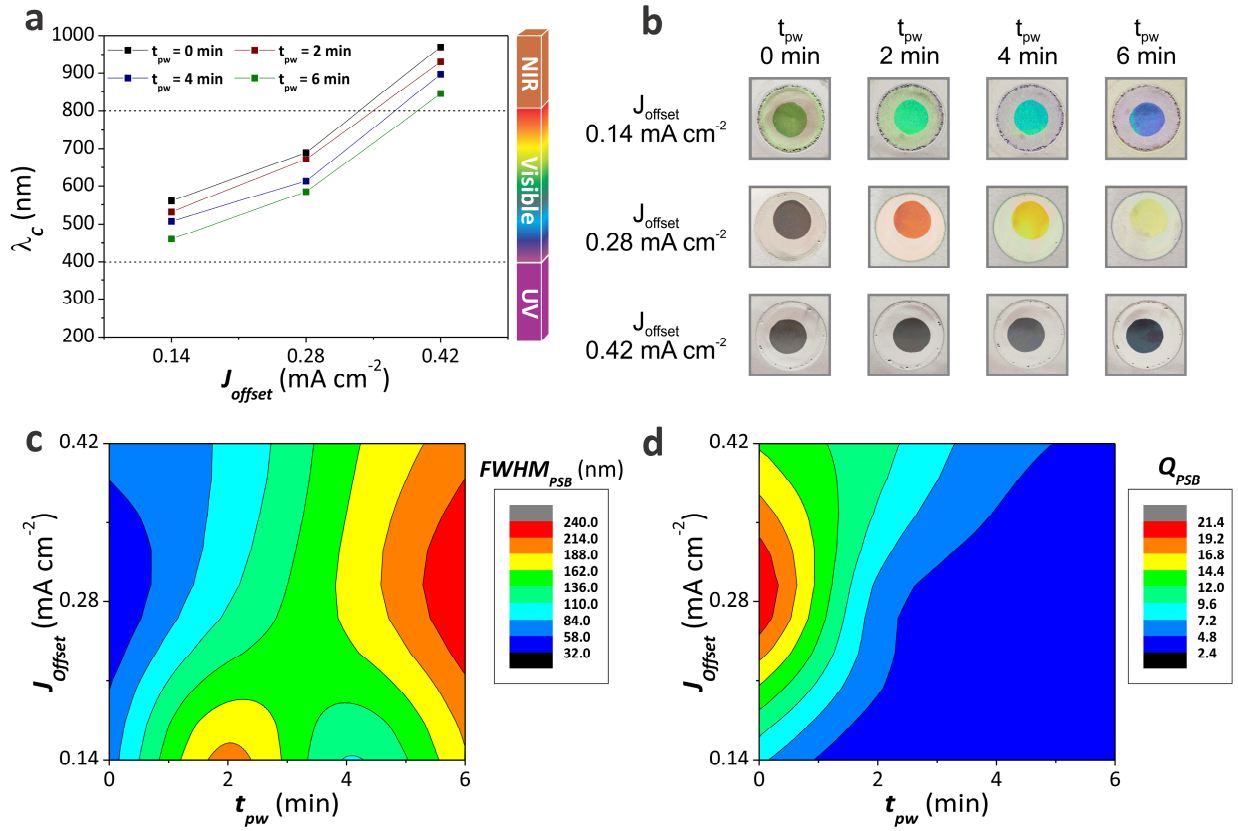

Figure 5. Effect of J_{offset} on the transmission features of logarithmic negative apodised NAA-DBRs. (a) A linear distribution of λ_c of apodised NAA-DBRs as a function of J_{offset} and t_{pw} across the UV-visible-NIR spectrum. (b) Digital photos establishing the colour characteristics of apodised NAA-DBRs with diameter of 1 cm resulting from the effect of J_{offset} and t_{pw}. (c) Dependence of $FWHM_{PSB}$ on J_{offset} and t_{pw} for apodised NAA-DBRs. (d) Dependence of Q_{PSB} of apodised NAA-DBRs as a function of J_{offset} and tpw. (Note: ΔA_J and T_p were fixed at 0.21 mA cm^{-2} and 1300 s)

4. CONCLUSIONS

This study has successfully engineered NAA-based distributed Bragg reflectors by apodised stepwise pulse anodisation using a logarithmic negative function, where their transmission features such as quality and position of photonic stop bands and interferometric colours were systematically assessed. Apodisation based on logarithmic negative function is demonstrated to be effective in narrowing the bandwidth, increasing the intensity and reducing the characteristic sidelobes of the photonic stop bands of NAA-DBRs. Fabrication parameters such as apodisation amplitude difference, anodisation period, current density offset and pore widening time were modified to tune the transmission features of NAA-DBRS and optimise the quality of the photonic stop bands of NAA-DBRs. This study reveals that the manipulation of amplitude difference has a stronger effect on Q_{PSB} than $FWHM_{PSB}$ and λ_c, where the dependency of Q_{PSB} is particularly stronger when the apodisation amplitude difference is at 0.21 mA cm^{-2}. As for the effect of the anodisation period, a red shift in λ_c is observed when anodisation period is altered from 1100 to 1500 s. $FWHM_{PSB}$ has shown a diminished correlation to the anodisation period as compared to that of Q_{PSB}. NAA-DBRs with narrower bandwidth and better quality are produced when their anodisation period is optimised at 1300 s. In addition to that, the effect of increasing current density offset has established a red shift in λ_c. The effect of current density offset on Q_{PSB} is relatively weak, on the contrary, the dependence of Q_{PSB} is stronger and increases as the current density offset approaches 0.28 mA cm^{-2}. Through the systematic modifications of apodisation parameters, the highest value of Q_{PSB} apodised NAA-DBRs achieved is 21.3 ± 0.6, which is 3.5 times greater than apodised rugate filters and 4.1 times greater than non-apodised NAA-DBRs. Another parameter studied was the pore widening time, where it is found out that an increase in t_{pw} has the same effect on the transmission characteristic of NAA-DBRs such as a blue shift in λ_c, an increase in $FWHM_{PSB}$ as well as a decrease in Q_{PSB} regardless of the changing apodisation parameters. The broadening effect on the characteristic bands of NAA-DBRs due to pore widening treatment may enhance the intensity of the characteristics band, but it is unfavourable for the production of narrow line-width NAA-DBRs. Furthermore, NAA-DBRs are demonstrated to display vivid colours across the spectral regions such as green, blue, red, orange and yellow that corresponds to their position of λ_c across UV-visible-NIR spectrum. It is worthwhile to note that among the fabrication parameters assessed in this study, apodisation amplitude difference has a more significant effect on Q_{PSB} of NAA-DBRs, and thus it is a more effective parameter in optimising Q_{PSB}. On the other hand, the fine and precise tuning of λ_c and interferometric colours of NAA-DBRs across the spectrum can be achieved by the manipulation of anodisation period and current density offset. To conclude, this study establishes the use of apodisation as an effective approach to tune the filtering features of NAA-based photonic structures, which could have broad applicability in different fields and disciplines such as sensing and biosensing.

ACKNOWLEDGEMENTS

Authors thank the support provided by the Australian Research Council (ARC) through the grant number DE140100549 and the School of Chemical Engineering (UoA). Authors thank the Adelaide Microscopy (AM) centre for FEG-SEM characterization.

REFERENCES

[1] Santos, A., "Nanoporous anodic alumina photonic crystals: fundamentals, developments and perspectives," J. Mater. Chem. C 5, 5581-5599 (2017).
[2] López. C., "Materials aspects of photonic crystals," Adv. Mater. 15(20), 1679-1704 (2003).
[3] Akahane, Y., Asano, T., Song, B-S. and Noda, S., "High-Q photonic nanocavity in a two-dimensional photonic crystal," Nature, 425(6961), 944-947 (2003).
[4] Noda, S., Tomoda, K., Chutinan, A., and Yamamoto, N., "Full three-dimensional photonic bandgap crystals at near-infrared wavelengths," Science 289 (5479), 604-606 (2000).
[5] Noda, S., Chutinan, A. and Imada, M., "Trapping and emission of photons by a single defect in a photonic bandgap structure," Nature 407 (6804), 608-610 (2000).
[6] Song, B-S., Noda, S., Asano, T., and Akahane, Y., "Ultra high-Q photonic double heterostructure nanocavity," Nat. Mat. 4(3), 207-210 (2005).

[7] Yablonovitch, E., "Inhibited spontaneous emission in solid-state physics and electronics," Phys. Rev. Lett. 58(20), 2059-2062 (1987).
[8] Yablonovitch, E., "Photonic band-gap structures," J. Opt. Soc. Am. B 10(2), 283-295 (1993).
[9] Charlton, M. D. B., Roberts, S. W. and Parker, G. J., "Guided mode analysis, and fabrication of a 2-dimensional visible photonic band structure confined within a planar semiconductor waveguide," Mater. Sci. Eng. B. 49(2), 155-165 (1997).
[10] Gerard, J. M., Izrael, A., Marzon, J. Y., Padjen, R. and Laan, F. R., "Photonic bandgap of two-dimensional dielectric crystals," Solid-State Electron 37(4), 1341-1344 (1994).
[11] Berger, V., Gauthier-Lafaye, O. and Coastard, E., "Fabrication of a 2D photonic bandgap by a holographic method," Electron. Lett. 33(5), 425-426 (1997).
[12] Yi-Yan, A., Wilkinson, C. D. and Laybourn, P. J., "Two-dimensional grating unit cell demultiplexer for thin-film optical waveguide," IEEE J. Quantum Electron. 16, 1089-1092 (1980).
[13] Zengerle, R., "Light propagation in singly and doubly periodic planar waveguides," J. Mod. Opt. 34(12), 1589-1617 (1987).
[14] Little, B. E., Foresi, J. S., Steinmeyer, G., Theon, E. R., Chu, S. T., Haus, H. A., Ippen, E. P., Kimerling, L. C. and Greene, W., "Ultra-compact Si-SiO_2 microring resonator optical channel dropping filters," IEEE Photonics Technol. Lett. 10(4), 549-551 (1998).
[15] Scherer, A., Painter, O., d'Urso, B., Lee, R. and Yariv, A., "InGaAsP photonic band gap crystal membrane microresonators," J. Vac. Sci. Technol. B 16(6), 3906-3910 (1998).
[16] Tonucci, R., Justus, B. L., Campillo, A. J. and Ford, C. E., "Nanochannel glass array," Science 258, 783-785 (1992).
[17] Lawandy, N. M., Balachandran, R. M., Gomes, A. S. L. and Sauvain, E., "Laser action in strongly scattering media," Nature 368(6470), 436-438 (1994).
[18] Holland, B. T., Blanford, C. F., and Stein, A., "Synthesis of macroporous minerals with highly ordered three-dimensional arrays of spheroidal voids," Science 281 (5376), 538– 540 (1998).
[19] Grüning, U., Lehmann, V., Ottow, S. and Busch, K., "Macroporous silicon with a complete two-dimensional photonic band gap centered at 5 μM," Appl. Phys. Lett. 68(6), 747-749 (1996).
[20] Grüning, U., Lehmann, V. and Engelhardt, C. M., "Two-dimensional infrared photonic band gap structure based on porous silicon," Appl. Phys. Lett 66(24), 3254-3256 (1995).
[21] Rowson, S., Chelnokov, A., Cuisin, C. and Lourtioz, J. M., "Three-dimensional characterization of a two-dimensional photonic bandgap reflector at midinfrared wavelengths," IEE Proc.: Optoelectron 145(6), 403-408 (1998).
[22] Lau, H. W., Parker. G. J., Greef, R. and Hölling, M., "High aspect ratio submicron pillars fabricated by photoassisted electrochemical etching and oxidation," Appl. Phys. Lett. 67(13), 1877-1879 (1995).
[23] Ishikura, N., Fuijii, M., Nishida, K., Hayashi, S., and Diener, J., "Porous silicon based extended-bandwidth rugate filters for mid-infrared application," Infrared Phys. Technol. 53(4), 292-294 (2010).
[24] Kumeria, T., Mohammad Mahbubur, R., Santos, A., Ferré-Borrul, J., Marsal, L.F. and Losic, D., "Nanoporous anodic alumina rugate filters for sensing of ionic mercury: towards environmental point-of-analysis systems," ACS Appl. Mater. Interfaces 6(15), 12971-12978 (2014).
[25] King, B. and Sailor, M. J., "Medium-wavelength infrared gas sensing with electrochemically fabricated porous silicon optical rugate filters," J. Nanophoton. 5(1), 051510 (2011).
[26] Pavesi, L., "Porous silicon dielectric multilayers and microcavities," L. Riv. Nuovo Cim. 20(1), 1-75 (1997)
[27] Salem, M. S., Ibrahim, S. M. and Amin, M., "Facile design and stabilization of a novel one-dimensional silicon-based photonic crystal microcavity," J. Appl. Phys. 122(3), 033104 (2017).
[28] Hotta, K., Yamaguchi, A. and Terramae, N., "Nanoporous waveguide sensor with optimized nanoarchitectures for highly sensitive label-free biosensing," ACS Nano 6(2), 1541-1547 (2012).
[29] Loni, A., Canham, L., Berger, M., Arens-Fischer, R., Munder, H., Luth, H., Arrand, H. and Benson, T., "Porous silicon multilayer optical waveguides," Thin Solid Films 276(1), 143-146 (1996).
[30] Argawal, V. and Del Rio, J., "Tailoring the photonic band gap of a porous silicon dielectric mirror," Appl. Phys. Lett. 82(10), 1512-1514 (2003).
[31] Chen, Y., Santos, A., Wang, Y., Kumeria, T., Ho, D., Li, J., Wang, C. and Losic, D., "Rational design of photonic dust from nanoporous anodic alumina films: a versatile photonic nanotool for visual sensing," Sci. Rep. 5, 12893 (2015).

[32] Losic, D. and Santos, A., [Nanoporous anodic alumina: fabrication, structure, properties and applications], Springer, Switzerland (2015).
[33] Busch, K., Lölkes, S., Wehrspohn, R. B., Föll, H., [Photonic crystals: advances in design, fabrication, and characterization], Wiley-VCH Verlag GmbH &Co. KGaA, Weinheim, 63-84 (2006).
[34] Santos, A., Kumeria, T., Wang, Y. and Losic, D., "In situ monitored engineering of inverted nanoporous anodic alumina funnels: on the precise generation of 3D optical nanostructures," Nanoscale 6, 9991-9999 (2014).
[35] Santos, A., Balderrama, V. S., Alba, M., Formentín, P., Ferré-Borrull, J., Pallarès, J. and Marsal, L. F., "Nanoporous anodic alumina barcodes: toward smart optical biosensors," Adv. Mat. 24(12)., 1050-1054 (2012).
[36] Kumeria, T., Mohammad Mahbubur, R., Santos, A., Ferré-Borrul, J., Marsal, L.F. and Losic, D., "Structural and optical nanoengineering of nanoporous anodic alumina rugate filters for real-time and label-free biosensing applications," Anal. Chem. 86(3), 1837-1844 (2014).
[37] Kumeria, T., Santos, A., Mohammad Mahbubur, R., Ferré-Borrul, J., Marsal, L.F. and Losic, D., "Advanced structural engineering of nanoporous photonic structures: tailoring nanopores architecture to enhance sensing properties," ACS Photonics 1(12), 1298-1306 (2014).
[38] Kumeria, T., Santos, A. and Losic, D., "Nanoporous anodic alumina platforms: engineered surface chemistry and structure for optical sensing applications," Sensors 14(7), 11878-11918 (2014).
[39] Kumeria, T., Santos, A. and Losic, D., "Ultrasensitive nanoporous interferometric sensor for label-free detection of gold (III) ions," ACS Appl. Mater. Interfaces 5(22), 11783-11790 (2013).
[40] Rahman, M. M., Marsal, L. F., Pallarès, J. and Ferré-Borrull, J., "Tuning the photonic stop bands of nanoporous anodic alumina-based distributed Bragg reflectors by pore widening," ACS Appl. Mater. Interfaces 5(24), 13375-13381(2013).
[41] Shang, G. L., Fei, G. T., Zhang, Y., Yan, P., Xu, S. H. and Zhang, L. D., "Preparation of narrow photonic bandgaps located in the near infrared region and their applications in ethanol gas sensing," J. Mater. Chem. C 1, 5285-5291(2013).
[42] Santos, A., Kumeria. T. and Losic, D., "Nanoporous anodic alumina: a versatile platform for optical biosensors," Materials 7(6), 4297-4320 (2014).
[43] Santos, A., Kumeria. T. and Losic, D., "Nanoporous anodic aluminum oxide for chemical sensing and biosensors," Trends Anal. Chem. 44, 25-38 (2013).
[44] Chen, Y., Santos, A., Ho, D., Wang, T., Kumeria, T., Li, J., Wang, C. and Losic, D., "On the generation of interferometric colors in high purity and technical grade aluminum: an alternative green process for metal finishing industry," Electrochim. Acta 174, 672-681 (2015).
[45] Wang, Y., Chen, Y., Kumeria, T., Ding, F., Evdokiou, A., Losic, D. and Santos, A., "Facile synthesis of optical microcavities by a rationally designed anodisation approach: tailoring photonic signals by nanopores structure," ACS Appl. Mater. Interfaces 7(18), 9879-9888. (2015).
[46] Santos, A., Kumeria, T. and Losic, D., "Optically optimized photoluminescent and interferometric biosensors based on nanoporous anodic alumina: a comparison," Anal. Chem. 85(16), 7904-7911 (2013).
[47] Macias, G., Ferré-Borrul, J., Pallarès, J. and Marsal, L.F, "1-D nanoporous anodic alumina rugate filters by means of small current variations for real-time sensing applications," Nanoscale Res. Lett. 9(1), 1-6 (2014).
[48] Macias, G., Hernández-Eguía, L. P., Ferré-Borrull, J., Pallarès, J. and L. F. Marsal, "Gold-coated ordered nanoporous anodic alumina bilayers for future label-free interferometric biosensors," ACS Appl. Mater. Interfaces 5(16), 8093-8098 (2013).
[49] Zheng, W. J., Fei, G. T., Wang, B., Jin, Z. and Zhang, D. L., "Distributed Bragg reflector made of anodic alumina membrane," Mater. Lett. 63(8), 706-708 (2009).
[50] Xu, Q., Sun, H-Y., Yang, Y-H., Liu, L-H. and Li, Z-Y., "Optical properties and color generation mechanism of porous anodic alumina films," Appl. Surf. Sci. 258(5), 1826-1830 (2011).
[51] Liu, Y., Wang, H. H., Indacochea, J. E. and Wang, M. L., "A colorimetric sensor based on anodized aluminum oxide (AAO) substrate for the detection of nitroaromatics," Sens. Actuators B160(1), 1149-1158 (2011).
[52] Wang, B., Fei, G. T., Wang, M., Kong, M. G. and Zhang, L. D., "Preparation of photonic crystals made of air pores in anodic alumina," Nanotechnology 18(36), 365601 (2007).
[53] Chen, Y., Santos, A., Wang, Y., Kumeria, T., Wang, C., Li, J. and Losic, D., "Interferometric nanoporous anodic alumina photonic coatings for optical sensing," Nanoscale 7(17), 7770-7779 (2015).
[54] Yao, Z., Zheng, M., Ma, L. and Shen, W., "The fabrication of ordered nanoporous metal films based on high field anodic alumina and their selected transmission enhancement," Nanotechnology 19(46), 465705 (2008).

[55] Santos, A., Pereira, T., Law, C. S. and Losic, D., "Rational engineering of nanoporous anodic alumina optical bandpass filters," Nanoscale 8(31), 14846-14857 (2016).
[56] Sukarno, Law, C. S. and Santos, A., "Realisation and optical engineering of linear bandpass filters in nanoporous anodic alumina photonic crystals," Nanoscale 9(22), 7541-7550 (2017).
[57] Law, C. S., Santos, A., Nemati, M. and Losic, D., "Structural engineering of nanoporous anodic alumina photonic crystals by sawtooth-like pulse anodisation," ACS Appl. Mater. Interfaces 8(21), 13542-13554 (2016).
[58] Santos, A., Law, C.S., Lei, D. W. C., Pereira, T. and Losic, D., "Fine tuning of optical signals in nanoporous anodic alumina photonic crystals by apodized sinusoidal pulse anodisation," Anal. Chem. 88(11), 5971-5980 (2016).
[59] Santos, A., Law, C.S., Pereira, T. and Losic, D., "Nanoporous hard data: optical encoding of information within nanoporous anodic alumina photonic crystals," Nanoscale 8(15), 8091-8100 (2016).
[60] Santos, A., Yoo, J. H., Rohatgi, C. V., Kumeria, T., Wang, Y. and Losic, D., "Realisation and advanced engineering of true optical rugate filters based on nanoporous anodic alumina by sinusoidal pulse anodisation," Nanoscale 8(3), 1360-1373 (2016).
[61] Lorenzo, E., Oton, C. J., Capuj, N. E., Ghulinyan, M., Navarro-Urrios, D., Gaburro, Z. and Pavesi, L., "Porous silicon-based rugate filters," Appl. Opt. 44(26), 5415-5421 (2005).
[62] Ilyas, S., Böcking, T., Killian, K., Reece, P. J., Gooding, J., Gaus, K. and Gal, M., "Porous silicon based narrow line-width rugate filters," Opt. Mater. 29(6), 619-622 (2007).
[63] Rahman, M., Garcia-Caurel, E., Santos, A., Marsal, L., Pallarès, J. and Ferré-Borrull, J., "Effect of anodization voltage on the pore-widening rate of nanoporous anodic alumina," Nanoscale Res. Lett. 7(1), 1-7 (2012).